6.2

VORTEX INTERACTIONS AND THE BAROTROPIC ASPECTS OF CONCENTRIC EYEWALL FORMATION

H.-C. Kuo *
National Taiwan University, Taipei, Taiwan
W. H. Schubert
Colorado State University, Fort Collins, Colorado

1. INTRODUCTION

The general interaction of two vorticity patches with the same vorticity, but with different horizontal areas, has been described by Dritschel and Waugh (1992). Based on a quantification of the final to initial circulation of each vortex, the interactions can be classified into five different types: elastic interaction, partial straining out, complete straining out, partial merger, and complete merger. There are many tropical cyclone observations that resemble these binary vortex interaction regimes (e.g., see Kuo et al. 2000, Prieto et al. 2003). In the complete straining out regime the smaller vortex is drawn out into thin filaments of vorticity surrounding the larger vortex, with no incorporation of fluid into the large vortex. This regime resembles the concentric vorticity structure of tropical cyclones, except the vorticity filaments are probably too thin to be called a concentric eyewall. Observations of Typhoon Lekima (Kuo et al. 2004, hereafter K04) indicate that it had a large area of convection with weak cyclonic vorticity outside the core vortex and that this weak vorticity wrapped around the inner eyewall on a time scale of 12 hours. This scenario can be idealized as the binary interaction of a small and strong vortex (the tropical cyclone core) with a large and weak vortex (the vorticity induced by moist convection outside the core vortex). This type of binary interaction was not studied by Dritschel and Waugh, since their vortices were assumed to have the same strength and their larger vortex was always the "victor." With the introduction of a "vorticity strength parameter" into the binary interaction problem with Rankine vortices, K04 added a third dimension to the Dritschel-Waugh parameter space and two new types of resulting interaction: concentric vorticity structure and tripole vorticity structure. A tripole is a linear arrangement of three regions of distributed vorticity of alternate signs, with the whole configuration steadily rotating in the same sense as the vorticity of the elliptically shaped central core (Carton et al. 1989, Polvani and Carton 1990, Carton and Legras 1994, Kloosterziel and Carnevale 1999). Examples of elliptical eyes that resemble a tripole vortex structure were reported by Kuo et al. (1999) for the case of Typhoon Herb (1996), and by Reasor et al. (2000) for the case of Hurricane Olivia (1994).

Based on the arguments of Okubo (1970) and Weiss (1991), Rozoff et al. (2006, hereafter R06) examined the rapid filamentation zones that form in intense tropical cyclones. They pointed out that the strain-dominated flow region just outside the radius of maximum wind of the core vortex can contribute significantly to the moat dynamics. Namely, the strong differential rotation outside the radius of maximum wind of the core vortex may also contribute to the formation and maintenance of the moat. They also note that one way to produce a concentric vorticity structure is through the interaction between a strong core vortex and a background turbulent vorticity field. The vorticity halo produced in their experiment, however, has only half the magnitude of that produced in typical binary vortex interactions. The effect of vorticity skirts on binary vortex interaction and the effect of turbulent background vorticity on the formation of concentric vorticity structures are the focal points of this paper. The paper extends the work of K04 and R06 by including an extended vorticity gradient outside the radius of maximum wind in the binary vortex interaction as well as by exploring the concentric eyewall formation in a turbulent background vorticity with various characteristic spatial scales. Passive microwave observations of secondary eyewall formation are presented in section 2. Section 3 describes the solution method and the model parameters. Section 4 gives the model results. The summary and concluding remarks are given in section 5.

2. PASSIVE MICROWAVE OBSERVATIONS OF SECONDARY EYEWALL FORMATION

From a study of passive microwave data

* *Corresponding author address:* H.-C. Kuo, Dept. of Atmospheric Science, National Taiwan University, Taipei, Taiwan; e-mail: kuo@lanczos.as.ntu.edu.tw

from 1997 to 2002, Hawkins and Helveston (2004) concluded that concentric eyewalls exist in a much higher percentage of tropical cyclones than previously estimated from visible and infrared satellite sensors. Although based on a small sample, their results suggest that approximately 40% of the Atlantic, 60% of the Eastern Pacific, and 80% of the Western Pacific intense storms (maximum wind $\geqq$ 120 knots) have concentric eyewalls. Figure 1 shows 3 western Pacific storms with concentric eyewalls, as viewed with passive microwave sensors. The data are from the Naval Research Laboratory Marine Meteorology Division in Monterey, CA (NRL-MRY) (Hawkins et al., 2001). In each case, the time period shown is approximately 12 hours. Initially the deep convection, indicated by the brown color, tends to be quite asymmetric with respect to the core and to possess random turbulent features.

In Typhoons Imbudo, Dujuan, and Maemi, a large area of convection outside the core vortex appears to wrap around the inner eyewall to form a concentric eyewall. The initial separation distance of the outer deep convection region from the vortex core varies from case to case. For example, the outer deep convection almost touches the vortex core in Typhoon Dujuan, while the outer deep convection is some 100 km away from the vortex core in Typhoon Maemi. Figure 1 suggests that a symmetric structure can evolve from asymmetric convection on a time scale of approximately 12 hours. The microwave imagery also illustrates moats of different sizes in the concentric eyewall cases. Even though the initial separation distances are different in Typhoons Imbudo, Dujuan, and Maemi, the concentric eyewalls possess a value of approximately unity for the ratio of moat width to core radius. In contrast, the largest moat is found in Typhoon Winnie, with its outer eyewall at a radius of 275 km (Zhang et al. 2005), which yields a value of 6 for the ratio of moat width to core radius.

The explanation of an interaction over such a large distance requires an extension of the previous binary vortex interaction results of K04, who studied only vortices with sharp edges (i.e. unskirted vortices). It should be noted that vorticity skirts play a role in other aspects of tropical cyclone dynamics. For example, DeMaria and Chan (1984) argued that mergers in binary vortex interaction can also occur due to vortex propagation on the outer vorticity gradients associated with each vortex. The interaction of the tangential wind field with the outer vorticity field of the companion vortex adds a component to the motion that can cause the separation distance to either decrease or increase, depending on the direction of the vorticity gradient. A vortex with a negative radial gradient of vorticity will be more merger-prone. Moreover, the slower decrease of angular velocity associated with the extended vorticity field should slow the filamentation process and thus the moat formation.

Mallen et al. (2005) examined the swirling wind structure of tropical cyclones by utilizing flight-level observations collected from Atlantic and eastern Pacific storms during 1977—1999. Their results indicate that tropical cyclone structure is characterized by a relatively slow tangential wind decrease outside the radius of maximum wind and a corresponding skirt of significant cyclonic relative vorticity. The Rankine vortices used in K04 have zero vorticity outside the radius of maximum wind and hence a rapid decrease of angular velocity with radius outside the core.

3. NONDIVERGENT BAROTROPIC MODEL

The basic dynamics considered here is two-dimensional, nondivergent, barotropic with ordinary diffusion in a double periodic domain. The discretization of the model is based on the Fourier pseudospectral method, with 512 by 512 equally spaced collocation points on a 300 km by 300 km domain. The code was run with a dealiased calculation of quadratic nonlinear terms with 170 Fourier modes in each direction. Time differencing was via the fourth-order Runge-Kutta method with a 3 second time step. The diffusion coefficient, unless otherwise specified, was chosen to be $\nu = 6.5\ m^2s^{-1}$. For the 300 km by 300 km domain this value of ν gives an e^{-1} damping time of 3.37 hours for all modes having total wave number 170, and a damping time of 13.5 hours for modes having total wave number 85. Some of the experiments were repeated at increased resolution and/or with a larger domain size. From these experiments we conclude that the results shown here are insensitive to the domain size and to the resolution employed. Obviously, the use of so simple a model precludes the simulation of the complete secondary eyewall cycle, but it allows for some simple numerical experiments concerning the initial organizational processes involved in secondary eyewall formation.

We consider an initial condition consisting of two distinct vortices—a strong, skirted, core vortex and a weaker, larger, unskirted companion. The initial condition contains the six parameters ζ_1, ζ_2, R_1, R_2, d, α, where the ζ_1, ζ_2 are the vorticity field, R_1, R_2 the measure of

vortex size, d the distance between the center, and α the skirt parameter. The initial vorticity field is given by

$$\zeta(x,y,0)=\zeta_1\begin{cases}1, & \text{if } 0\le r_1\le 0.65,\\ c_0+c_1r_1+c_2r_1^{\,2}+c_3r_1^{\,3}, & \text{if } 0.65\le r_1\le 0.81,\\ \frac{1}{2}(1-\alpha)r_1^{\,-\alpha-1}, & \text{if } 0.81\le r_1\le\infty,\end{cases} \quad (1)$$
$$+\zeta_2\begin{cases}1\text{-}\exp\left[-\frac{30}{r_2}\exp\left(\frac{1}{r_2-1}\right)\right], & \text{if } 0\le r_2\le 1,\\ 0, & \text{if } 1\le r_2\le\infty,\end{cases}$$

The four constants (c_0, c_1, c_2, c_3) are determined by requiring continuity of the vorticity and its radial derivative at r_1 = 0.65 and r_1 = 0.81, where r_1 is nondimensional radius. To set the spatial and time scales to values relevant for tropical cyclones, we choose the initial maximum vorticity of the companion vortex to be ζ_2 = 3×10^{-3} s^{-1} and the size of the intense skirted core vortex to be R_1 = 10 km. This reduces the number of parameters to four, which we take to be the vorticity strength ratio $\gamma = \zeta_1/\zeta_2$, the vortex radius ratio r = R_1/R_2, the dimensionless gap $\Delta/R_1 = (d - R_1 - R_2)/R_1$ and the skirt parameter α.

The skirt parameter α allows the tangential wind outside of radius of maximum wind decay $r_1^{-\alpha}$. Note that the $\alpha = 1$ gives the Rankine vortex structure. Aircraft observations of the azimuthal winds in hurricanes (e.g., Shea and Gray 1973, Mallen et al. 2005) suggest that a reasonable range for the skirt parameter is $0.5\leqq\alpha\leqq1$. It is important to note that the vorticity skirt on the core vortex provides two important new effects to the previous K04 arguments, which were based on initial unskirted vortices. First, the radial vorticity gradient associated with the vorticity skirt provides a means by which vortex Rossby waves can propagate (Montgomery and Kallenbach 1997, Balmforth et al. 2001). Secondly, the vorticity in the skirt region of the strong vortex can contribute significantly to the circulation at the radius of the companion vortex, especially when the skirt parameter α is small. For example, the vorticity in the central region and the vorticity in the skirt region make approximately equal contributions to the circulation at r_1 = 3 in the case α = 0.7, while the contribution from the skirt region is actually larger than the contribution from the central region in the case α = 0.5.

4. MODEL RESULTS

Figure 2 gives vorticity field for binary vortex interactions with respect to skirt parameter $\alpha = 0.7$, vorticity strength ratio $\gamma = 7$, radius ratio r = 1/4 and dimensionless gap Δ/R_1 = 5. Figure 3 depicts tangential wind speed along a radial emanating westward from the center of the strong core vortex for the experiment shown in Figure 1. The wind profiles clearly show a secondary maximum in the tangential wind field contracting with time. The secondary wind maximum increases from the initial 25 ms^{-1} to 40 ms^{-1} in 12 hours. The time and spatial scales of the secondary wind maximum contraction in Figure 3 are in general agreement with the observations in Hurricane Gilbert (Black and Willoughby 1992). The contraction mechanism for the outer bands is often argued to be a balanced response to an axisymmetric ring of convective heating (Shapiro and Willoughby 1982). The results shown in Figure 3 suggest that the nonlinear advective dynamics involved in the straining out of a large, weak vortex into a concentric vorticity band by a skirted core vortex can also result in contraction and in an increase of the secondary wind maximum. No moist convection is involved in the process. The moist convection, however, may give an additional enhancement of the strength of the outer band.

Figure 4 summarizes the binary interaction regimes as a function of the skirt parameter α, the dimensionless gap Δ/R_1 and the vorticity strength ratio γ for the radius ratios r = 1/4. We have classified the interactions using the scheme devised by Dritschel and Waugh (1992) and extended by K04. The five categories are (i) Elastic Interaction, (ii) Merger, (iii) Straining-out, (iv) Tripole, and (v) Concentric. The abscissa in the two-dimensional parameter space of Figure 4 is the dimensionless gap Δ/R_1, which ranges from 0 to 6, and the ordinate is the vorticity strength ratio γ, which ranges from 4 to 10. The α = 1 cases are reproduced from Fig.~10 of K04, with the addition of the results from the Δ/R_1= 5, 6 experiments to the diagram.

Figure 4 indicates that, when the companion vortex is large (r =1/4), the α = 0.7 and α = 0.5 vortices produce concentric structures in the region where the Rankine vortex has elastic interaction (i.e., $\Delta/R_1 \geqq 4$). The α = 0.7 vortex produces mainly concentric structure for $\Delta/R_1\geqq 4$, while the α = 0.5 vortex produces straining-out when core vortex is strong (i.e., γ is large). Of particular interest is the fact that the formation of concentric vorticity structures for α = 0.5 and α = 0.7 requires a separation distance that is four times the core vortex radius. The Rankine vortex produces a concentric vorticity structure when the separation distance is within three to four times the core vortex radius. Thus, it is conceivable that a core vortex of sufficient strength can form a concentric vorticity structure at large radius through binary vortex interaction. This is consistent with satellite microwave observations that suggest a wide range of possible radii for concentric eyewalls.

Our simulations suggest that concentric vorticity structures can result from binary interactions involving a skirted core vortex. The strong core vortex provides a flow field that strains out the weaker vortex into a thin strip of enhanced vorticity wrapped around the core vortex at a larger distance than allowed by an unskirted core vortex. A neighboring vorticity area that is three or four times the core vortex radius is required for a binary vortex interaction with skirts to form a concentric structure. Tripole structures occur in the region of parameter space separating the merger and the concentric regimes. The regime diagrams indicate that a Rankine vortex favors the formation of a concentric structure closer to the core vortex, while the α=0.7 and α=0.5 vortices favor the formation of concentric structures farther from the core vortex.

We now address the question of whether the rapid development of a strong vortex within a chaotic background vorticity field can lead to concentric vorticity patterns similar to those observed during binary vortex interactions. R06 used a core vortex that approximates a Category 5 hurricane 75 ms^{-1} tangential winds near 25 km radius) embedded within turbulent background vorticity elements having horizontal scales between 20 km and 40 km. Their results (e.g., their Fig.~8) indicate the formation of a concentric structure, but with the magnitude of the outer vorticity ring much weaker than the one resulting from binary vortex interactions. Our experiments extend those of R06 by using a wider range of the horizontal spatial scales and by including a vorticity clear zone (moat) near the core vortex. In real hurricanes the moat can be viewed as being the result of the strong subsidence induced just outside the eyewall by convection within the eyewall (e.g., Dodge et al. 1999). Presumably, the moat produced by the strong subsidence associated with eyewall convection should be present in our large γ experiments. We have simply imposed a 10 km or 20 km wide moat in the initial condition.

Figure 5 depicts the initial conditions and t = 24 hr model results with the background turbulent vorticity parameters r* = 3 and r* = 6 (the background turbulent vorticity characteristic scales of 20—30 km and 50—60 km respectively) and with the vortex strength parameters γ = 6 and γ = 10. Experiments with no moat, a 10 km moat, and a 20 km moat were performed.

These results suggest that a concentric eyewall structure with $\zeta \sim 10^{-3}$ s^{-1} can form in the presence of the moat. In agreement with R06, the case with r* = 3 and γ = 10 yields a concentric structure with $\zeta \sim 10^{-4}$ s^{-1}. It is interesting to note the formation of triple eyewalls in the experiment with r* = 3, γ = 10 and a 10 km wide moat. A triple eyewall, as revealed by 85 GHz satellite data in Hurricane Juliette, was recently reported by McNoldy (2004). The experiments with moats also yield outer vorticity bands with similar strength. On the other hand, when the background turbulent vorticity possesses characteristic scales of 50—60 km (i.e., r* = 6), the experiments with 10 km and 20 km wide moats yield concentric vorticity structures with $\zeta \sim 10^{-3}$ s^{-1}, which are similar in magnitude to those produced in binary vortex interaction.

Figure 6 summarizes the end states for background turbulent experiments as a function of the turbulent spatial scale parameter r* and the vorticity strength ratio γ for the no-moat, 10 km moat and 20 km moat scenarios. We have classified the resulting interactions using a scheme similar to Figure 4, but with the inclusion of the triple concentric eyewall case (Tri-C). Concentric vorticity structures are favored when γ is greater than 4. Figure 6 suggests that stronger core vortices (in general $\gamma \geqq 4$), larger spatial scale in background turbulent vorticity (r* $\geqq$ 2), and the presence of the moat favor the formation of the concentric vorticity regime. Note that the concentric structures in the no-moat experiments are often a magnitude smaller in vorticity strength. Moat experiments with r* $\geqq$ 5 yield outer bands with vorticity strength similar to the binary vortex interaction.

5. SUMMARY

Passive microwave data suggest the common presence of large areas of asymmetric deep convection and random turbulent convective structures some 12 hours before the formation of concentric eyewalls. As an idealization of the interaction of a tropical cyclone core with a large region of nearby weaker vorticity, the authors consider nondivergent barotropic model integrations of the binary interactions of modified Rankine vortices, which are vortices with a uniform high vorticity core surrounded by a vorticity skirt. An important parameter in the classification of the resulting interactions is the vorticity strength ratio. Variation of this parameter can lead to end states that can be classified as tripole structures, concentric eyewall structures, or multiple eyewall structures. Concentric vorticity structures result from binary interactions in which the small, core vortex is 4 to 6 times stronger than the larger companion vortex. An additional requirement is that the separation distance between the edges

of the two vortices be less than 6 times the core vortex radius. A core vortex with a vorticity skirt results in the formation of an outer band at radii larger than three times the core vortex radius. Moreover, for the formation of concentric structures from initally skirted vortices, the outer vortex radius is required to be at least three times larger than the core vortex radius. The numerical results also indicate that a strong tropical cyclone with a moat of 10—20 km width is able to organize a stirred vorticity field with 40—50 km spatial scale into a concentric structure similar to those formed in binary vortex interactions. Both the binary vortex interaction experiments and the turbulent background vorticity experiments highlight the pivotal role of the core vorticity strength in maintaining itself, in stretching, organizing and stabilizing the outer vorticity field, as well as the shielding effect of the moat in preventing further merger and enstrophy cascade processes during concentric eyewall formation. Finally, the results support the notion that concentric eyewalls form only in strong tropical cyclones. Our results, along with those of Dodge et al. (1999) and R06, suggest that the subsidence, the straining out caused entrainment to the convections, and advection and axisymmetrization of negative vorticity anomaly associated with a strong core vortex may all contribute to the formation of the moat.

In closing we note that the appearance of tripoles in the present study adds to a long list of ways in which these structures can be produced. For example, tripoles emerge from unstable initial states in laboratory experiments with both rotating fluids (Kloosterziel and van Heijst 1991, van Heijst et al. 1991, Denoix et al. 1994) and pure electron plasmas (Driscoll and Fine 1990), as coherent structures in two-dimensional turbulence simulations (Legras et al. 1988), as the result of collisions of two dipoles (Larichev and Reznik 1983, Orlandi and van Heijst 1992), as a result of finite amplitude quadrapolar (i.e., azimuthal wavenumber 2) distortions of a monopolar Gaussian vorticity distribution (Rossi et al. 1997), as a result of the barotropic instability across the annular region separating a strong core vortex from a weaker vorticity ring (Kossin et al. 2000), and as the end state of an initial vorticity distribution in which a low vorticity eye is uncentered within a region of high vorticity (Prieto et al. 2001). Given their robustness and multitude of production methods, we might ask the question: Do tripoles actually play a role in tropical cyclone dynamics? Unfortunately, our in situ measurement techniques, which involve aircraft flight legs in only a few radial directions, do not provide sufficient data to compute a potential vorticity (or even a vorticity) field that would reveal a tripole structure, if it were present. Thus, a critical need is observational methods that would provide much finer scale analyses (particularly in the azimuthal direction) of the vorticity and potential vorticity fields. Perhaps airborne Doppler radar will eventually provide such data. In any event, because tripole structures are so robust and can be produced in so many different ways, it would be surprising if they did not play some role in tropical cyclone dynamics. If they are eventually observed in hurricanes, it will be an indication of incomplete mixing in the hurricane core, since, from statistical mechanics arguments, tripoles are a restricted statistical equilibrium far from the limit of strong mixing (Robert and Rosier 1997, Chavanis and Sommeria 1998).

REFERENCES

Balmforth, N. J., S. G. Llewellyn Smith, and W. R. Young, 2001: Disturbing vortices. *J. Fluid Mech.*, **426**, 95-133.

Black, M. L., and H. E. Willoughby, 1992: The concentric eyewall cycle of Hurricane Gilbert. *Mon. Wea. Rev.*, **120**, 947-957.

Carton, X., G. R. Flierl, and L. M. Polvani, 1989: The generation of tripoles from unstable axisymmetric isolated vortex structure. *Europhys. Lett.*, **9**, 339-344.

Carton, X., and B. Legras, 1994: The life-cycle of tripoles in two-dimensional incompressible flows. *J. Fluid Mech.*, **267**, 53-82.

Chavanis, P. H., and J. Sommeria, 1998: Classification of robust isolated vortices in two-dimensional hydrodynamics. *J. Fluid Mech.*, **356**, 259-296.

DeMaria, M., and J. C. L. Chan, 1984: Comments on “A numerical study of the interactions between two tropical cyclones.” *Mon. Wea. Rev.*, **112**, 1643-1645.

Denoix, M.-A., J. Sommeria, and A. Thess, 1994: Two-dimensional turbulence: The prediction of coherent structures by statistical mechanics. *Progress in Turbulence Research*, H. Branover and Y. Unger, Eds., AIAA, 88-107.

Dodge, P., R. W. Burpee, and F. D. Marks Jr., 1999: The kinematic structure of a hurricane with sea level pressure less than 900 mb. *Mon. Wea. Rev.*, **127**, 987-1004.

Driscoll, C. F., and K. S. Fine, 1990: Experiments on vortex dynamics in pure electron plasmas. *Phys. Fluids*, **2**, 1359-1366.

Dritschel, D. G., and D. W. Waugh, 1992: Quantification of the inelastic interaction of unequal vortices in two-dimensional vortex

dynamics. *Phys. Fluids*, **A4**, 1737-1744.

Hawkins, J. D., and M. Helveston, 2004: Tropical cyclone multiple eyewall characteristics. Preprints, 26th Conference on Hurricanes and Tropical Meteorology, Miami Beach, FL, Amer. Meteor. Soc., 276-277.

Hawkins, J. D., T. F. Lee, J. Turk, C. Sampson, J. Kent, and K. Richardson, 2001: Real-time internet distribution of satellite products for tropical cyclone reconnaissance. *Bull. Amer. Meteor. Soc.*, **82**, 567-578.

Kloosterziel, R. C., and G. F. Carnevale, 1999: On the evolution and saturation of instabilities of two-dimensional isolated circular vortices. *J. Fluid Mech.*, **388**, 217-257.

Kloosterziel, R. C., and G. J. F. van Heijst, 1991: An experimental study of unstable barotropic vortices in a rotating fluid. *J. Fluid Mech.*, **223**, 1-24.

Kossin, J. P., W. H. Schubert, and M. T. Montgomery, 2000: Unstable interactions between a hurricane's primary eyewall and a secondary ring of enhanced vorticity. *J. Atmos. Sci.*, **57**, 3893-3917.

Kuo, H.-C., R. T. Williams, and J.-H. Chen, 1999: A possible mechanism for the eye rotation of Typhoon Herb. *J. Atmos. Sci.*, **56**, 1659-1673.

Kuo, H.-C., G. T.-J. Chen, and C.-H. Lin, 2000: Merger of tropical cyclones Zeb and Alex. *Mon. Wea. Rev.*, **128**, 2967-2975.

Kuo, H.-C., L.-Y. Lin, C.-P. Chang, and R. T. Williams, 2004: The formation of concentric vorticity structures in typhoons. *J. Atmos. Sci.*, **61**, 2722-2734.

Larichev, V. D., and G. M. Reznik, 1983: On collisions between two-dimensional solitary Rossby waves. *Oceanology*, **23**, 545-552.

Legras, B., P. Santangelo, and R. Benzi, 1988: High resolution numerical experiments for forced two-dimensional turbulence. *Europhys. Lett.*, **5**, 37-42.

Mallen, K. J., M. T. Montgomery, and B. Wang, 2005: Reexamining the near-core radial structure of the tropical cyclone primary circulation: Implications for vortex resiliency. *J. Atmos. Sci.*, **62**, 408-425.

McNoldy, B. D., 2004: Triple eyewall in Hurricane Juliette. *Bull. Amer. Meteor. Soc.*, **85**, 1663-1666.

Montgomery, M. T., and R. J. Kallenbach, 1997: A theory for vortex Rossby-waves and its application to spiral bands and intensity changes in hurricane. *Quart. J. Roy. Meteor. Soc.*, **123**, 435-465.

Okubo, A., 1970: Horizontal dispersion of floatable particles in the vicinity of velocity singularities such as convergences. *Deep-Sea Res.*, **17**, 445-454.

Orlandi, P., and G. J. F. van Heijst, 1992: Numerical simulations of tripolar vortices in 2d flow. *Fluid Dyn. Res.*, **9**, 179-206.

Polvani L. M., and X. J. Carton, 1990: The tripole: A new coherent vortex structure of incompressible two-dimensional flows. *Geophys. Astrophys. Fluid Dyn.*, **51**, 87-102.

Prieto, R., J. P. Kossin, and W. H. Schubert, 2001: Symmetrization of lopsided vorticity monopoles and offset hurricane eyes. *Quart. J. Roy. Meteor. Soc.*, **127**, 1-17.

Prieto, R., B. D. McNoldy, S. R. Fulton, and W. H. Schubert, 2003: A classification of binary tropical-cyclone-like vortex interactions. *Mon. Wea. Rev.*, **131**, 2656-2666.

Reasor, P. D., M. T. Montgomery, F. D. Marks, and J. F. Gamache, 2000: Low-wavenumber structure and evolution of the hurricane inner core observed by airborne dual-Doppler radar. *Mon. Wea. Rev.*, **128**, 1653-1680.

Robert, R., and C. Rosier, 1997: The modeling of small scales in two-dimensional turbulent flows: A statistical mechanics approach. *J. Stat. Phys.*, **86**, 481-515.

Rossi, L. F., J. F. Lingevitch, and A. J. Bernoff, 1997: Quasi-steady monopole and tripole attractors for relaxing vortices. *Phys. Fluids*, **9**, 2329-2338.

Rozoff, C. M., W. H. Schubert, B. D. McNoldy, and J. P. Kossin, 2006: Rapid filamentation zones in intense tropical cyclones. *J. Atmos. Sci.*, **63**, 325-340.

Shapiro, L. J., and H. E. Willoughby, 1982: The response of balanced hurricanes to local sources of heat and momentum. *J. Atmos. Sci.*, **39**, 378-394.

Shea, D. J., and W. M. Gray, 1973: The hurricane's inner core region. I. Symmetric and asymmetric structure. *J. Atmos. Sci.*, **30**, 1544-1564.

van Heijst, G. J. R., R. C. Kloosterziel, and C. W. M. Williams, 1991: Laboratory experiments on the tripolar vortex in a rotating fluid. *J. Fluid Mech.*, **225**, 301-331.

Weiss, J., 1991: The dynamics of enstrophy transfer in two-dimensional hydrodynamics. *Physica D*, **48**, 273-294.

Zhang, Q.-H., S.-J. Chen, Y.-H. Kuo, K.-H. Lau, and R. A. Anthes, 2005: Numerical study of a typhoon with a large eye: Model simulation and verification. *Mon. Wea. Rev.*, **133**, 725-742.

2003-09W-IMBUDO

072012Z-130kts **0720-0942Z** | 072012Z-130kts **0720-1244Z** | 072100Z-130kts **0720-2219Z**

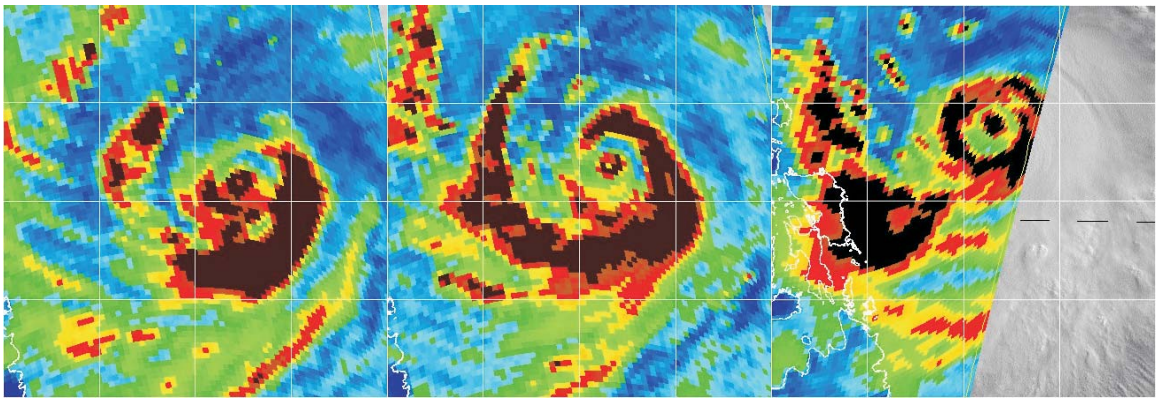

2003-14W-DUJUAN

083112Z-95kts **0831-1214Z** | 090100Z-120kts **0831-2235Z** | 090112Z-125kts **0901-0949Z**

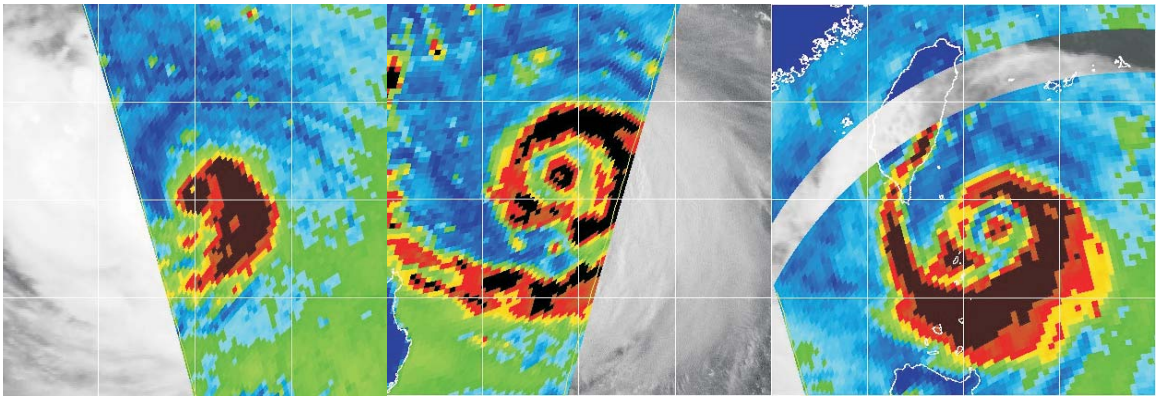

2003-15W-MAEMI

091000Z-150kts **0909-2209Z** | 091000Z-150kts **0909-2239Z** | 091012Z-150kts **0910-0925Z**

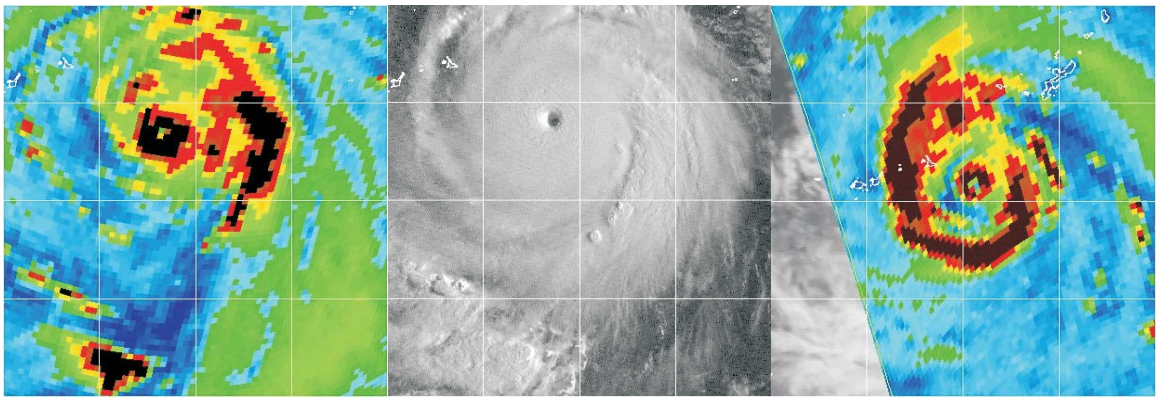

Figure 1. Passive microwave image sequences for 3 western Pacific typhoons with concentric eyewalls. For each typhoon the time interval is approximately 12 hours, and the estimated maximum winds are indicated at the top of the image.

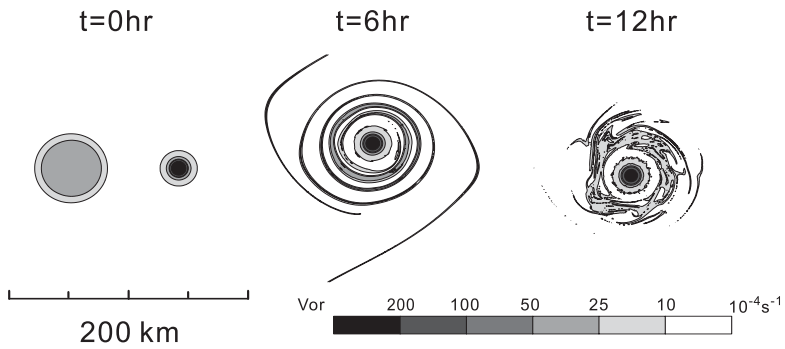

Figure 2. Vorticity field for binary vortex interactions with respect to α = 0.7, γ = 7, r = 1/4 and Δ/R_1 = 5.

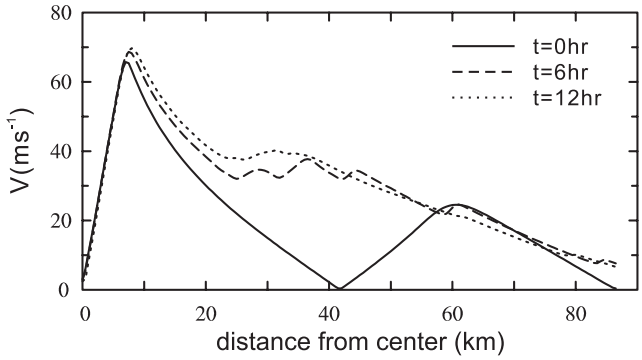

Figure 3. Tangential wind speed along a radial emanating westward from the center of the strong core vortex for the experiment shown in Figure 2.

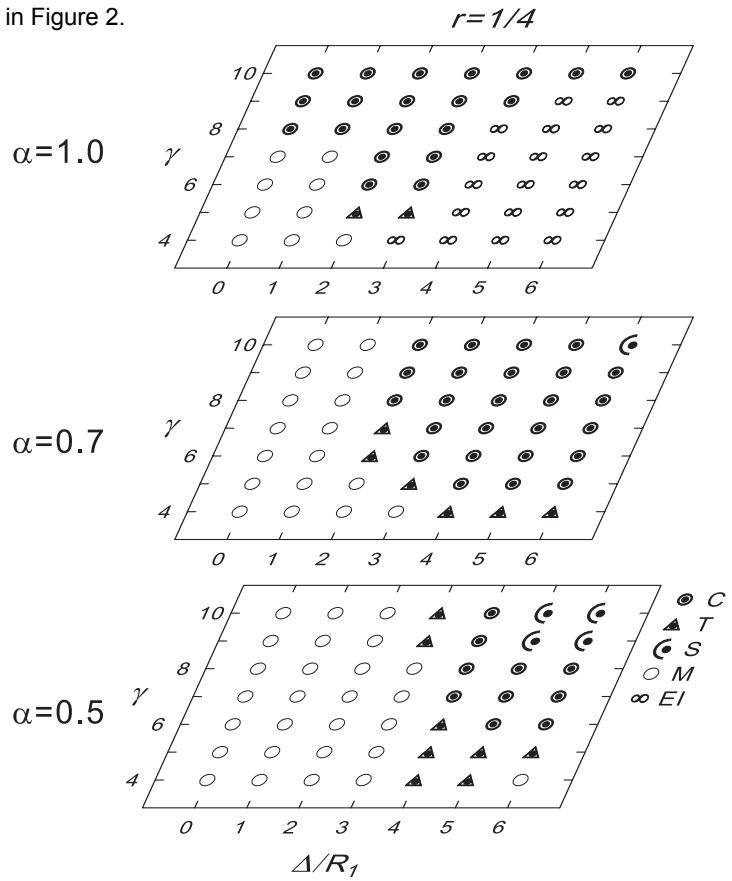

Figure 4. Summary of the binary interaction regimes as a function of the skirt parameter α, the dimensionless gap Δ/R_1, and the vorticity strength ratio $\gamma = \zeta_1/\zeta_2$ for the radius ratios $r = R_1/R_2$ = 1/4. As indicated by the code at lower right, the structures are categorized as follows: Elastic Interaction (EI), Merger (M), Straining out (S), Tripole (T), Concentric (C).

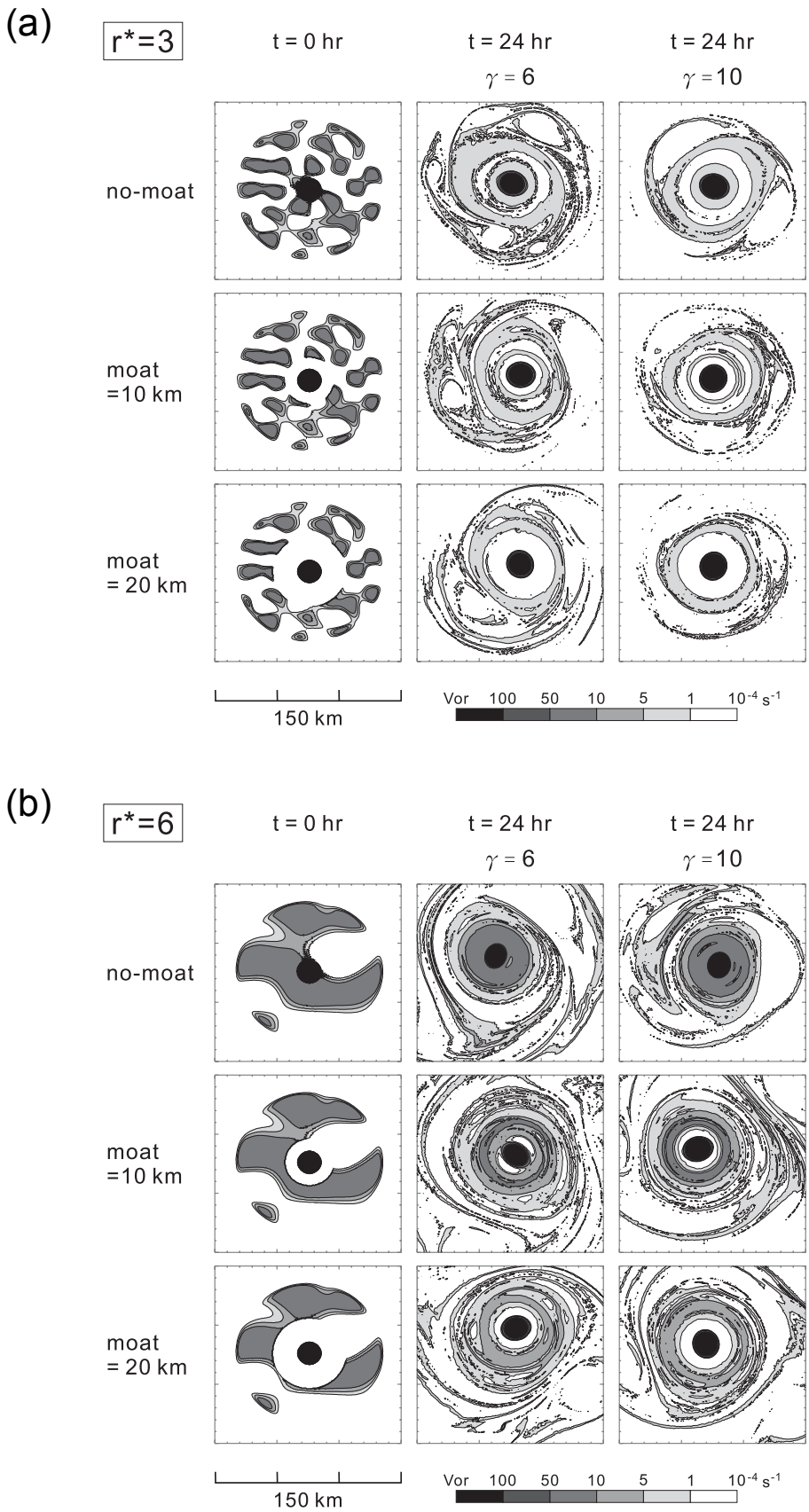

Figure 5. The initial conditions and t = 24 hr model results with the background turbulent vorticity parameters r* = 3 and r* = 6 (parts (a) and (b) respectively), and with the Rankine core vortex strength parameters γ = 6 and γ = 10. Experiments with no moat, a 10 km moat, and a 20 km moat are shown.

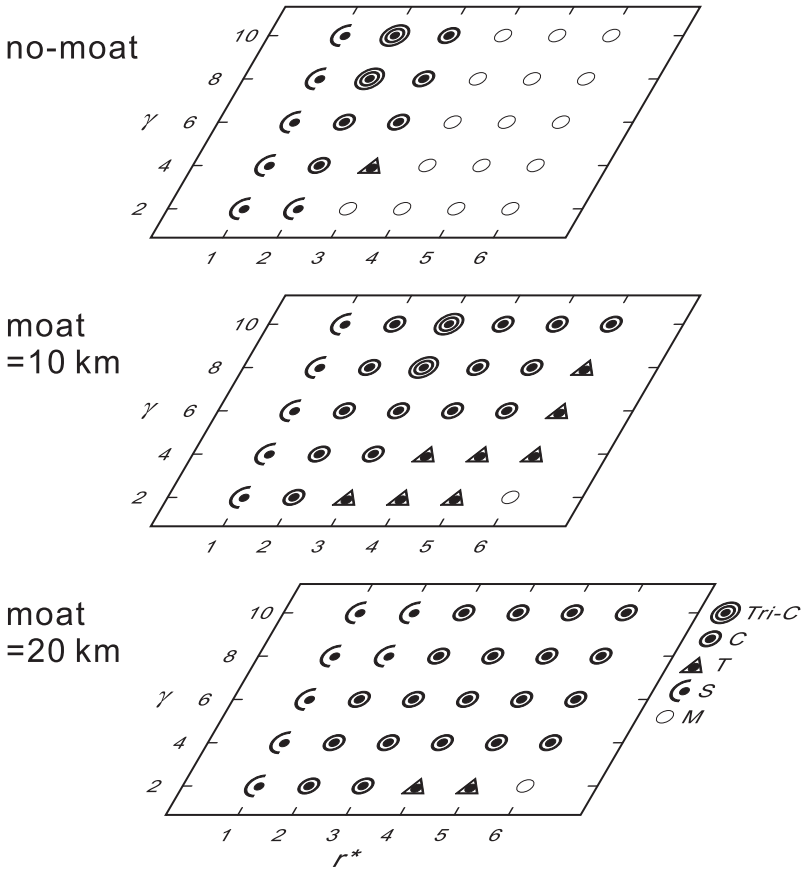

Figure 6. Interaction regimes for background turbulent experiments as a function of the turbulent spatial scale parameter r* and the vorticity strength ratio $\gamma = \zeta_1/\zeta_2$ for the no-moat, 10 km moat and 20 km moat scenarios. The code for interaction type is the same as in Figure 4, with the addition of triple concentric eyewall (Tri-C).